CHAPTER W10

Mechanical Properties of Materials

W10.1 Relationship of Hooke's Law to the Interatomic $U(r)$

Since the macroscopic deformation of a solid reflects the displacements of individual atoms from their equilibrium positions, it should not be surprising that the elastic response of a solid is determined by the nature of the interactions between neighboring atoms. In fact, Hooke's law can be derived from the form of the potential energy of interaction $U(r)$ for a pair of atoms, as shown for a pair of hydrogen atoms in Fig. 2.1 of the textbook.[†] The equilibrium separation of the two atoms corresponds to the minimum in the $U(r)$ curve at $r = r_0$. Since $U(r)$ is a continuous function, it can be expanded in a Taylor series about $r = r_0$, as follows:

$$U(r) = U(r_0) + (r - r_0)\left(\frac{dU}{dr}\right)_{r_0} + \frac{(r - r_0)^2}{2}\left(\frac{d^2U}{dr^2}\right)_{r_0} + \cdots. \tag{W10.1}$$

The first derivative, $(dU/dr)_{r_0}$, is equal to zero at the equilibrium separation $r = r_0$. In addition, cubic and other higher-order terms can be neglected since $(r - r_0) \ll r_0$ for the (typically) small displacements from equilibrium.

It follows that the force acting between a pair of atoms can be approximated by

$$F(r) = -\frac{dU(r)}{dr} = -(r - r_0)\left(\frac{d^2U}{dr^2}\right)_{r_0} = -k(r - r_0), \tag{W10.2}$$

where k is a constant. This result has the same form as Hooke's law since the displacement $(r - r_0)$ of atoms from their equilibrium positions is proportional to the restoring force F. This displacement is also inversely proportional to the curvature $(d^2U/dr^2)_{r_0}$ of the potential energy curve at $r = r_0$, which for a given material is a constant in a given direction.

It can be seen from Eqs. (10.21) and (W10.2) that *Young's modulus* E is proportional to the curvature $(d^2U/dr^2)_{r_0}$ of the potential energy. This is a reasonable result since the macroscopic deformations that correspond to the microscopic displacements of atoms from their equilibrium positions will be more difficult in materials where the potential energy well is deeper and hence $U(r)$ increases more rapidly as the atoms are displaced

[†] The material on this home page is supplemental to *The Physics and Chemistry of Materials* by Joel I. Gersten and Frederick W. Smith. Cross-references to material herein are prefixed by a "W"; cross-references to material in the textbook appear without the "W."

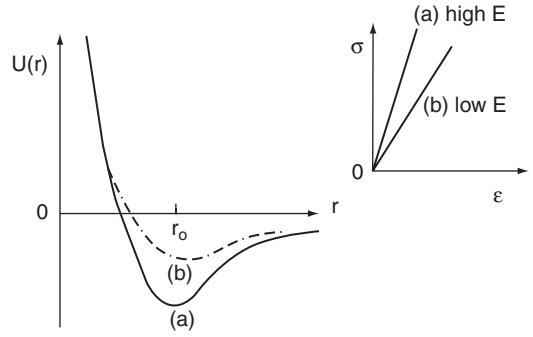

Figure W10.1. Schematic potential energies of interaction $U(r)$ for "deep" and "shallow" potential wells and corresponding stress–strain curves

from their equilibrium positions. This is illustrated schematically in Fig. W10.1 for the cases of "strong" and "weak" bonding between pairs of atoms, corresponding to "deep" and "shallow" potential wells, respectively. For the case of a material with strong bonding and a deep potential well, the curvature $(d^2U/dr^2)_{r_0}$ is high. Such a material will have a high stiffness E and a high slope for the initial linear portion of its stress–strain curve, as shown in the inset of this figure. The opposite will be true for a material having weak bonding, a shallow potential well, and a corresponding low curvature $(d^2U/dr^2)_{r_0}$. In this case the material will have a low stiffness E. It should be noted that the stress–strain curve will eventually become nonlinear as the stress increases, due to the nonparabolicity of the interatomic potential $U(r)$ for large displacements $(r - r_0)$.

Estimates for the magnitude of the elastic modulus E and its dependence on material properties can be obtained by noting that E, as a measure of the stiffness of a material, should be proportional to the stress needed to change the equilibrium separation between atoms in a solid.[†] For many materials with ionic, metallic, and covalent bonding, this stress is itself approximately proportional to the magnitude of the interatomic Coulomb force $F = q^2/4\pi\epsilon d^2$, where q is the ionic charge, d the interatomic separation, and ϵ the electric permittivity of the material. This stress should also be inversely proportional to the effective area, $\approx d^2$, over which the interatomic force acts. Thus the stress, and hence E, should be proportional to q^2/d^4.

A test of this relationship is presented in Fig. W10.2, where the bulk modulus B, defined in Section 10.6, is shown plotted as a function of the interatomic separation d in a logarithmic plot for three classes of materials with ionic, metallic, and covalent bonding, respectively. For each class of materials the measured values of B fall on a straight line with a slope close to -4, as predicted by the simple argument presented above. It is clear from this result that high elastic stiffness is favored in materials where the ions have large effective charges and are separated by small interatomic separations.

The magnitude of the elastic constants can also be estimated from the expression $E \approx q^2/4\pi\epsilon d^4$ by using $1/4\pi\epsilon \approx 9 \times 10^9$ N · m^2/C^2, $q = e = 1.6 \times 10^{-19}$ C, and $d \approx$

[†] See the discussion in Gilman (1969, pp. 29–42).

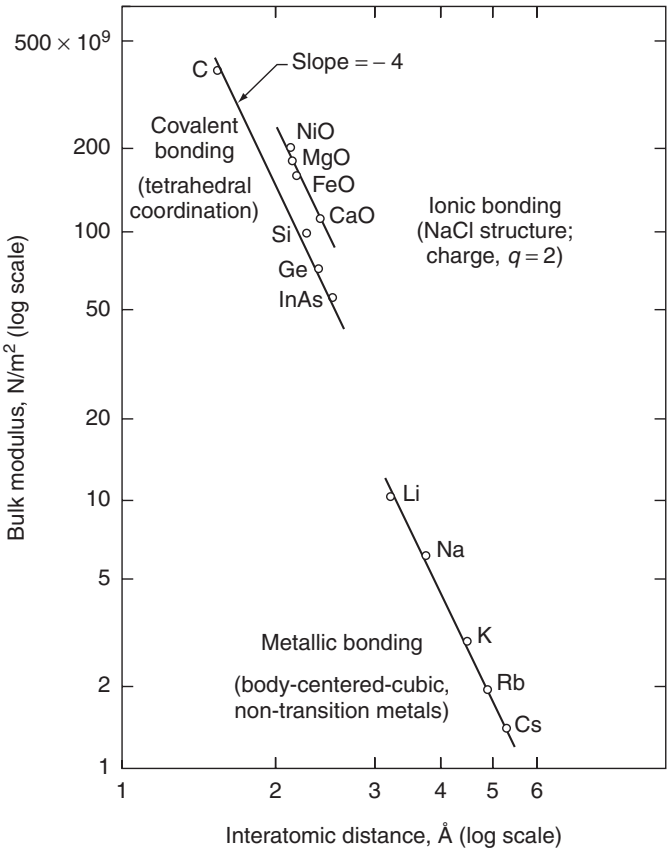

Figure W10.2. Logarithmic plot of the bulk modulus B versus the interatomic separation d for three classes of materials with ionic, metallic, and covalent bonding, respectively. (From A. G. Guy, *Introduction to Materials Science*, McGraw-Hill, New York, 1972. Reprinted by permission of the McGraw-Hill Companies.)

0.2 nm. The result obtained, $E \approx 100$ GPa, is consistent with the experimental values shown in Fig. W10.2 and listed in Table 10.2.

W10.2 Zener Model for Anelasticity

An interesting and useful model for describing anelastic processes has been proposed by Zener. This model deals with a *standard linear solid*, a solid in which the stress σ, the strain ε, and their first derivatives $\partial\sigma/\partial t$ and $\partial\varepsilon/\partial t$ are related to each other in a linear equation. Although Zener's model may not be sufficiently general to describe all types of anelastic effects, it is quite useful for the purpose of illustrating important general aspects of anelasticity.

In the Zener model the following equation is used to describe the anelastic effects illustrated in Fig. 10.9:

$$\sigma + \tau_\varepsilon \frac{\partial \sigma}{\partial t} = E_r \left(\varepsilon + \tau_\sigma \frac{\partial \varepsilon}{\partial t} \right). \tag{W10.3}$$

Here τ_ε is the time constant for the relaxation of stress under conditions of constant strain, and τ_σ is the time constant for relaxation of strain under conditions of constant stress.[†] The quantity E_r is the *relaxed elastic modulus*, that is, the stress/strain ratio σ/ε after all relaxation has occurred in the solid and when $\partial\sigma/\partial t$ and $\partial\varepsilon/\partial t$ are zero. If the changes in stress and strain in the material occur so rapidly (e.g., at sufficiently high frequencies) that relaxation cannot proceed to completion, it can be shown that the stress/strain ratio is given by the *unrelaxed elastic modulus* $E_u = E_r\tau_\sigma/\tau_\varepsilon$.

The solutions of Eq. (W10.3) for the conditions shown in Fig. 10.9*a* (i.e., after relaxation has occurred) are as follows:

$$\begin{aligned} &\sigma = \sigma_0 \text{ and } \partial\sigma/\partial t = 0: \qquad \varepsilon(t) = \varepsilon_\infty + (\varepsilon_0 - \varepsilon_\infty)e^{-t/\tau_\sigma}. \\ &\sigma = 0 \text{ and } \partial\sigma/\partial t = 0: \qquad \varepsilon(t) = \varepsilon_\infty e^{-t/\tau_\sigma}. \end{aligned} \tag{W10.4}$$

Here $\varepsilon_\infty = \sigma_0/E_r$. These expressions illustrate the kinetics to be expected for simple relaxation processes where the fraction of the relaxation completed in time t is $f(t) = 1 - e^{-t/\tau}$. Analogous equations can be derived for the time dependence of σ for the conditions shown in Fig. 10.9*b*.

The mechanical response of materials to dynamic conditions of stress and strain is of interest both for applications and for fundamental studies of anelasticity. Under dynamic conditions, stress and strain are often periodic functions of time, that is,

$$\sigma(t) = \sigma_0 e^{-i\omega t} \quad \text{and} \quad \varepsilon(t) = \varepsilon_0 e^{-i\omega t}, \tag{W10.5}$$

where the amplitudes σ_0 and ε_0 can be complex quantities. Upon substitution of $\sigma(t)$ and $\varepsilon(t)$, Eq. (W10.3) becomes

$$(1 - i\omega\tau_\varepsilon)\sigma_0 = E_r(1 - i\omega\tau_\sigma)\varepsilon_0. \tag{W10.6}$$

A *complex elastic modulus* E_c can then be defined as

$$E_c = \frac{E_r(1 - i\omega\tau_\sigma)}{1 - i\omega\tau_\varepsilon} = \frac{\sigma_0}{\varepsilon_0}. \tag{W10.7}$$

For a stress amplitude σ_0 that is real, this corresponds to a complex amplitude ε_0 for the strain.

Under dynamic conditions and due to either elastic aftereffects or strain relaxation, the strain ε will in general lag behind the stress σ by a phase angle ϕ (i.e., $\varepsilon(t) = \varepsilon_0 \exp[-i(\omega t - \phi)]$), whose tangent is given by

$$\tan\phi = \frac{\text{Im } E_c}{\text{Re } E_c} = \frac{\omega(\tau_\sigma - \tau_\varepsilon)}{1 + \omega^2\tau_\varepsilon\tau_\sigma}. \tag{W10.8}$$

The quantity $\tan\phi$, known as the *loss coefficient*, is often used as a measure of the magnitude of the *internal friction* or energy loss in a material. When $\tan\phi$ is small,

[†] While the use of a single relaxation time is appropriate for some materials, other materials, such as polymers, can have a large number of relaxation times, spanning many orders of magnitude.

it can be shown that $\tan\phi \approx \Delta U_{\rm el}/2\pi U_{\rm el} = 1/Q$, where $\Delta U_{\rm el}/U_{\rm el}$ is the fraction of elastic energy dissipated per oscillation. (Q is the *quality factor* of an electrical circuit, with $1/Q$ being a measure of energy dissipation.)

The predicted frequency dependence of the internal friction is illustrated in Fig. W10.3, where $\tan\phi$ is shown as a function of frequency, specifically $\omega(\tau_\sigma\tau_\varepsilon)^{1/2} = \omega\langle\tau\rangle$. It can be seen that $\tan\phi$ has a maximum value at $\omega\langle\tau\rangle = 1$ [i.e., at $\omega_{\max} = (\tau_\sigma\tau_\varepsilon)^{-1/2}$] and falls to zero for both $\omega \ll \omega_{\max}$ and $\omega \gg \omega_{\max}$. For low frequencies, $\omega \ll \omega_{\max}$, the solid is fully relaxed, the elastic modulus is E_r, and the internal friction is close to zero in the Zener model, since the strain has sufficient time to follow the applied stress (i.e., the phase angle $\phi \approx 0$). At high frequencies, $\omega \gg \omega_{\max}$, the solid is unrelaxed, the elastic modulus is E_u, and the internal friction is again close to zero.

Note that $E_u > E_r$ in Fig. W10.3, which follows from $\tau_\sigma > \tau_\varepsilon$. In this case the strain relaxes more slowly than the stress [see the definitions given earlier for τ_σ and τ_ε in Eq. (W10.3)]. It follows that the material will be stiffer at high frequencies than at low frequencies. The hysteresis loops for such material will actually be closed, straight lines with slopes given by E_r and E_u at very low and very high frequencies, respectively. Thus Hooke's law will be valid for $\omega \gg \omega_{\max}$ and $\omega \ll \omega_{\max}$. At $\omega = \omega_{\max}$ the hysteresis loop will have its maximum width and maximum area $\Delta U_{\rm el}$.

Zener has pointed out that although this model for a standard linear solid has several general features that are observed for real materials, it does not in fact correspond in detail to the behavior observed for any real solid. Nevertheless, measurements of internal friction as a function of frequency often show the behavior predicted by Zener's model, as shown in Fig. W10.4 for German silver, an alloy of Cu, Ni, and Zn.

W10.3 Typical Relaxation Times for Microscopic Processes

See Table W10.1, from which it can be seen that lattice vibrations, the motion of elastic waves, and the dissipation of heat are "fast" processes at $T \approx 300$ K, while the diffusion of interstitial atoms and the motion of grain boundaries can be considered to be "slow" processes.

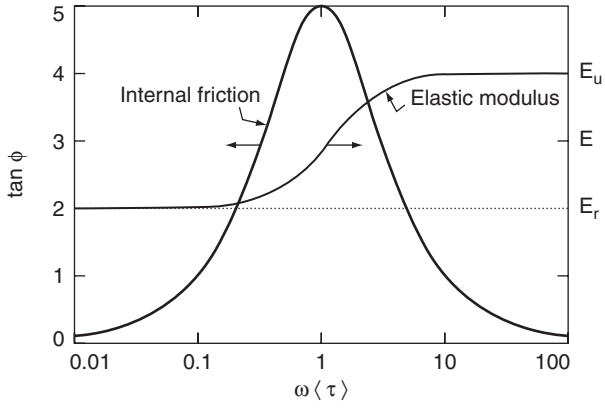

Figure W10.3. Magnitude of the internal friction $\tan\phi$ as a function of $\omega\langle\tau\rangle = \omega(\tau_\sigma\tau_\varepsilon)^{1/2}$. (Adapted from C. Zener, *Elasticity and Anelasticity of Metals*, University of Chicago Press, Chicago, 1948).

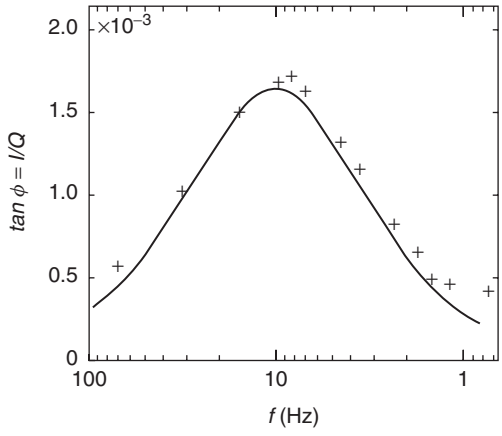

Figure W10.4. Magnitude of the internal friction $\tan\phi = 1/Q$ for German silver as a function of frequency. (From C. Zener, *Elasticity and Anelasticity of Metals*, University of Chicago Press, Chicago Copyright© 1948 by the University of Chicago. Reprinted by permission.)

TABLE W10.1 Typical Relaxation Times τ for Microscopic Processes in Solids at $T = 300$ K

Time Scale for τ (s)	Microscopic Process
10^{-14}	Electron collisions in metals
10^{-12}	Vibrations of atoms (lattice vibrations)
10^{-10}	
10^{-8}	Radiative recombination of electrons and holes
10^{-6}	
	Elastic wave traverses solid (as in brittle fracture)
10^{-4}	
	Dissipation of heat (thermal relaxation)
10^{-2}	
$10^{0} = 1$	
	(Time of typical tensile test $= t_{\text{test}}$)
10^{+2}	
10^{+4}	Diffusion of interstitial atoms
(1 week $\approx 6 \times 10^{5}$ s)	
10^{+6}	
(1 year $\approx 3 \times 10^{7}$ s)	Motion of grain boundaries
10^{+8}	Creep
	Flow of inorganic glasses

W10.4 Further Discussion of Work Hardening

The phenomenon of *work hardening* is difficult to treat theoretically, the most difficult aspect being to predict how the density and distribution of dislocations vary with the strain in the material. There is in fact no unique correlation between the level of strain and the resulting distribution of dislocations. The experimental situation is complicated by the fact that there can exist three distinct regions of work hardening when the plastic deformation is presented in the form of a shear stress–shear strain

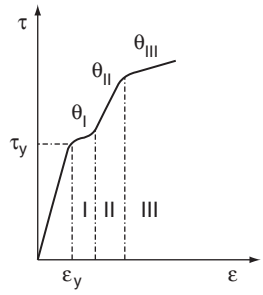

Figure W10.5. Shear stress–shear strain $\tau-\varepsilon$ curve for a typical single-crystal FCC metal. Three inelastic regions are shown, with the rate of work hardening in each region characterized by the slope $d\tau/d\varepsilon$, denoted by θ_{I}, θ_{II}, and θ_{III}, respectively

curve (i.e., τ versus ε). Such a curve is shown schematically in Fig. W10.5 for a typical FCC metal in the form of a single crystal. Beyond the elastic region which extends up to the *shear yield stress* τ_y, there can exist in some materials three inelastic regions, I, II, and III. The rate of work hardening in each region can be characterized by the slope $d\tau/d\varepsilon$, which is denoted by θ_{I}, θ_{II}, and θ_{III}, respectively. The higher the slope, the greater the rate at which work hardening occurs for a given increment in applied shear stress τ.

Although all may not be present in a given material, these regions have the following characteristics:

Region I. Plastic deformation in region I begins with the onset of "*easy glide*" or *slip* occurring on the primary slip system, as described in Section 10.14. A relatively low rate of work hardening occurs in region I. This region corresponds to the existence of long, straight slip lines in a single crystal. Region I is absent in polycrystals.

Region II. This is the linear work-hardening region, with $\theta_{\mathrm{II}} \approx 10\theta_{\mathrm{I}}$ and $\theta_{\mathrm{II}} \approx G/300$, where G is the shear modulus (i.e., the slope $d\tau/d\varepsilon$ in the elastic region). Plastic deformation in this region results in the interaction of dislocations and occurs via the mechanism of slip. The resulting distribution of dislocations is very inhomogeneous. The shear stress in region II is often observed to be proportional to the square root of the dislocation density ρ, that is,

$$\tau_y(\rho) = \tau_{y0} + \alpha G b\sqrt{\rho}. \tag{W10.9}$$

Here τ_{y0} is the shear yield stress (i.e., the shear stress needed to move a dislocation when no other dislocations are present), b is the Burgers vector, and α (≈ 0.3 to 0.6) is a constant. Note that ρ is given by the total length of all the dislocations divided by the volume of the material and has units of m^{-2}. It is clear from this expression that ρ is an increasing function of shear stress [i.e., $\tau_y(\rho) - \tau_{y0}$]. Typical values for single-crystal or polycrystalline Cu are $\rho \approx 10^{16}$ m^{-2} for $\tau_y \approx$ 100 MPa.

Region III. In this region the slope $d\tau/d\varepsilon$ decreases continuously with increasing stress, with the dependence of τ on ε usually observed to be close to parabolic, that is,

$$\tau(\varepsilon) = \theta_{\text{III}}\sqrt{\varepsilon - \varepsilon'}, \tag{W10.10}$$

where ε' is a constant.

Various theories can reproduce the form of Eq. (W10.9) observed in the linear region II or the parabolic dependence of τ on ε observed in region III. None of the theories of work hardening is completely satisfactory, however, which should not be surprising given the complexity of the problem. One of the first approaches, presented by Taylor, considered the source of work hardening to be the interactions between edge dislocations and the pinning that results. If l is the average distance that dislocations move before being pinned, the resulting shear strain ε corresponding to a dislocation density ρ is

$$\varepsilon = K\rho bl, \tag{W10.11}$$

where K is a constant that depends on orientation.

For a material containing a uniform distribution of edge dislocations, the average separation between the dislocations is $L \approx \rho^{-1/2}$. The applied shear stress required to move two dislocations past each other must overcome the effective internal stress acting on one dislocation due to the other. This can be written as

$$\tau = \frac{kGb}{L}, \tag{W10.12}$$

where k is a constant. Since $L \approx \rho^{-1/2}$, it follows that

$$\tau \approx kGb\sqrt{\rho}, \tag{W10.13}$$

which has the form of Eq. (W10.9). When Eqs. (W10.11) and (W10.13) are combined, the following dependence of τ on ε is obtained:

$$\tau(\varepsilon) \approx kG\sqrt{\frac{b\varepsilon}{Kl}} \approx k'G\sqrt{\frac{\varepsilon}{l}}, \tag{W10.14}$$

where k' is another constant. This prediction corresponds to the parabolic dependence of τ on ε observed in region III. The predictions of Taylor's theory therefore agree with the observed dependencies of τ on ρ and on ε despite the simplifying assumptions made, including the assumption of a uniform distribution of edge dislocations. Taylor's theory does not, however, explain the linear work hardening observed in region II.

W10.5 Strengthening Mechanisms

Dispersion Strengthening. *Dispersion strengthening* is a process in which small particles of a hard phase such as alumina (Al_2O_3) or silica (SiO_2) are distributed uniformly in the matrix of a weaker material (e.g., a copper alloy), either by precipitation in situ or by sintering the materials together. This process strengthens the

weaker host material and increases its resistance to plastic deformation. Dispersion-strengthened materials can have high hardness at high temperatures when the dispersed particles are of a refractory nature and very hard. This is an advantage of this strengthening method over precipitation hardening. The Orowan expression relating the yield stress σ_y to the interparticle spacing Λ is described in Chapter W21 with regard to the dispersion strengthening of steels

Precipitation Hardening. *Precipitation hardening* is a process in which a second phase is precipitated from a supersaturated solid solution in a matrix via heat treatment. Important examples include the precipitation of particles of Fe_3C or Fe_4N in iron and of particles of the intermetallic compound $CuAl_2$ in Al, as described in detail in Chapter W21. Both dispersion strengthening and precipitation hardening arise from short-range interactions between dislocations and the dispersed particles or the precipitate. As a result, the dislocations are pinned and cannot move freely through the material. The Orowan expression mentioned earlier is also applicable to these short-range interactions between dislocations and precipitate particles.

Long-range interactions between precipitate particles and dislocations are also possible due to the internal stresses created by the difference in average atomic volumes of the precipitate and the host matrix. Mott and Nabarro obtained the following estimate for the average shear strain ε_{av} in a single crystal due to a volume fraction f of spherical precipitate particles:

$$\varepsilon_{\text{av}} = 2\varepsilon f. \tag{W10.15}$$

Here $\varepsilon = \Delta r/r_0 = (r - r_0)/r_0$ is the fractional radial misfit resulting from the insertion of a particle of radius r in a cavity of radius $r_0 < r$ within the host matrix. The resulting strain leads to an increase in the critical shear yield stress by the amount

$$\Delta\tau_y = G\varepsilon_{\text{av}} = 2G\varepsilon f, \tag{W10.16}$$

where G is the shear modulus. According to this prediction, the critical shear yield stress should be independent of the particle sizes and interparticle separations. In fact, the precipitate particles will have little effect on the motion of the dislocations when the particles are small and closely spaced and also when they are large and far apart. Only at intermediate sizes and separations will they have a strong effect.

Solid-Solution Strengthening. An example of *solid-solution strengthening* is doubling of the yield strength of Fe–C solid-solution alloys at a C/Fe atom ratio of only $1/10^4$. As mentioned in Section 10.12, interstitial C atoms in octahedral sites cause tetragonal distortions of the BCC crystal structure of α-Fe. These lattice distortions in turn impede the motion of dislocations, thereby strengthening the Fe. This strengthening mechanism is described further for the case of steels in Chapter W21.

W10.6 Creep Testing

Typical creep tests at $0.5T_m < T < T_m$ and constant applied stress are shown in Fig. W10.6, where three distinct stages are shown for the dependence of the nominal strain on time. Results are shown at two applied stresses σ. It can be seen that the creep rate $\partial\varepsilon/\partial t$ is an increasing function of σ, as expected, and also of temperature T.

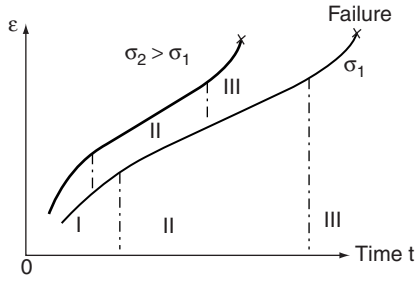

Figure W10.6. Typical creep test for $0.5T_m < T < T_m$ and constant applied stress. Three distinct stages are evident for the dependence of the nominal strain ε on time.

In stage I of *primary* creep the creep strain rate $\partial\varepsilon/\partial t$ actually slows down, probably as a result of work hardening, and reaches a value that typically remains constant in the most important stage II of *secondary* or *quasiviscous* creep. In stage III of *tertiary* creep the creep rate increases, nonuniform deformation begins, and failure eventually occurs. The *creep strength* of a material can be defined as the stress that will produce a given strain in a given time at a given temperature T. For example, a typical low-carbon nickel alloy has a creep strength of 60 MPa for $10^{-3}\%$ elongation per hour at $T = 534°\text{C}$. The stress for fracture σ_f due to creep is lower the longer the time of loading. Extrapolation of the results of creep tests to longer times is required for predicting the performance of materials in service (e.g., predicting when failure will occur under a given load or stress condition). This is due to the fact that creep tests generally do not extend to the point of failure, particularly when carried out at low stress levels and low temperatures.

Various models have been proposed to describe the dependencies of creep or the creep rate $\dot{\varepsilon} = \partial\varepsilon/\partial t$ on time, temperature, and stress. There is no universal model, but expressions such as

$$\varepsilon(t) = \varepsilon_0 + \varepsilon_p(1 - e^{-mt}) + \dot{\varepsilon}_s t, \tag{W10.17}$$

$$\frac{\partial\varepsilon}{\partial t} = A\sigma^n \exp\left(-\frac{Q_c}{k_B T}\right) \tag{W10.18}$$

have been proposed. In Eq. (W10.17), ε_0 is the initial strain in the material, the second term describes creep in stage I, and the term $\dot{\varepsilon}_s t$ (which is linear in time) represents stage II. Equation (W10.18) is proposed to be valid for the secondary creep rate in stage II, with A and n being constants and Q_c the thermal activation energy for creep. For a number of pure metals it has been found that $n = 5$ and that $Q_c \approx E_a(\text{diff})$, the measured thermal activation energy for self-diffusion in the metal.

A useful way of graphically illustrating the stress and temperature regions in which various deformation mechanisms are dominant (i.e., rate controlling) is the *Weertman–Ashby map*, shown in Fig. W10.7 for pure nickel. This map presents a plot of normalized tensile stress σ/G (where G is the shear modulus) versus T/T_m and corresponds to a critical strain rate $\dot{\varepsilon}_c$ of 10^{-8} s^{-1}. *Coble creep* and *Nabarro creep* correspond to diffusion of vacancies within the boundaries of the grains and within the bulk of the grains, respectively, and can be seen in Fig. W10.7 to be dominant in different regimes of temperature and stress.

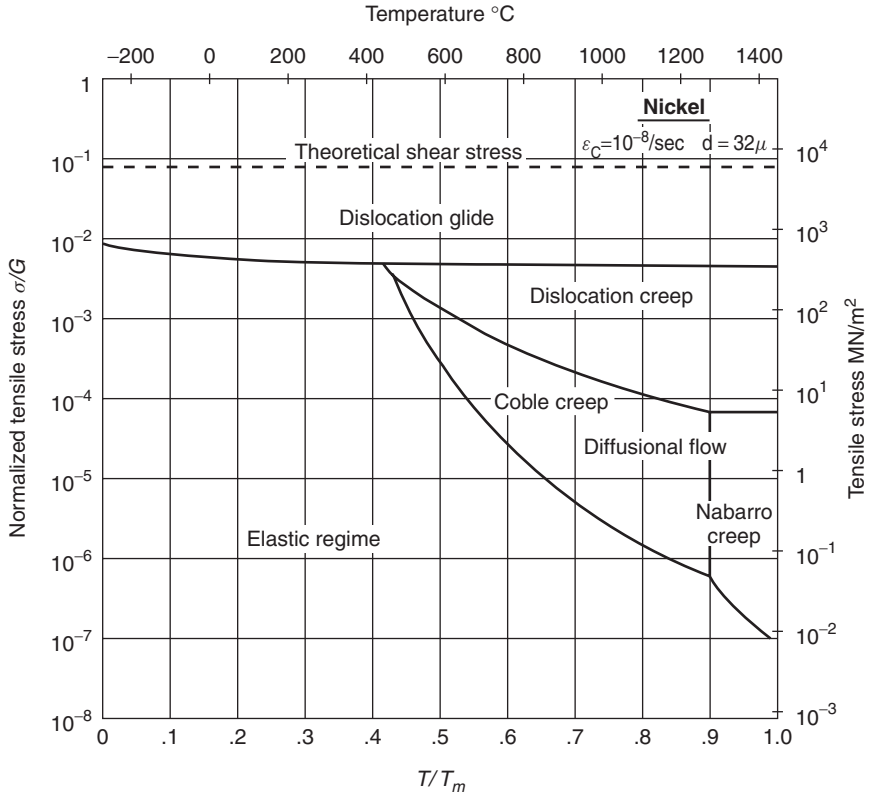

Figure W10.7. The Weertman–Ashby map presented here for pure nickel is a semilogarithmic plot of normalized tensile stress σ/G versus T/T_m for a critical strain rate $\dot{\varepsilon}_c$ of 10^{-8} s^{-1}. (Reprinted from *Acta Metallurgica*, Vol. 20, M. F. Ashby, p. 887. Copyright © 1972, by permission from Elsevier Science.)

W10.7 Further Discussion of Fatigue

When fatigue occurs under conditions of low true-stress amplitude σ_a, the response of the material is primarily elastic and the number of cycles to failure N_f is large. In this case the range $\Delta\varepsilon_e$ over which the elastic component of the strain varies can be described by

$$\Delta\varepsilon_e = \frac{2\sigma_a}{E} = \frac{2\sigma'_f}{E}(2N_f)^b, \tag{W10.19}$$

where b is the fatigue strength exponent and σ'_f is the fatigue strength coefficient, equal to the stress intercept for $2N_f = 1$. The quantity σ'_f is approximately equal to σ_f, the fracture stress under monotonic loading. The exponent b can be expressed in terms of the cyclic hardening coefficient n' by

$$b = -\frac{n'}{1+5n'}. \tag{W10.20}$$

Fatigue life thus increases with decreasing $|b|$, i.e. decreasing n'.

When fatigue occurs under conditions of higher stress amplitude σ_a and the response of the material has an inelastic or plastic component, the number of cycles to failure N_f will be smaller. The range of variation $\Delta\varepsilon_p$ of the plastic strain component can be described by the *Manson–Coffin relation*,

$$\Delta\varepsilon_p = 2\varepsilon'_f(2N_f)^c, \tag{W10.21}$$

where ε'_f, the ductility coefficient in fatigue, is equal to the strain intercept for $2N_f = 1$, and c is the ductility exponent in fatigue. Smaller values of c correspond to longer fatigue life. In the limit of high strain and low number of cycles c is given by

$$c = -\frac{1}{1+5n'}. \tag{W10.22}$$

As a result, fatigue life in this limit increases with increasing n'.

When a material is subjected under cyclic loading to both elastic and plastic strain, the fatigue strength will be determined by the total strain:

$$\Delta\varepsilon_t = \Delta\varepsilon_e + \Delta\varepsilon_p = \frac{2\sigma'_f}{E}(2N_f)^b + 2\varepsilon'_f(2N_f)^c. \tag{W10.23}$$

The separation of a $\Delta\varepsilon_t - N_f$ curve into its elastic and plastic components is illustrated schematically in Fig. W10.8. It can be seen that $\Delta\varepsilon_t$ approaches the plastic curve at high strain levels and the elastic curve at low strain levels.

W10.8 Hardness Testing

Hardness is often measured by the indentation of a harder material, typically a diamond indenter, into a softer material or by a scratch test. Indentation methods can be quantitative, while scratch testing gives essentially qualitative results. The most common methods of indentation hardness testing include the *Brinnell* and *Rockwell* tests and microindentation or microhardness tests such as the *Knoop* and *Vickers* tests. Hardness values are expressed using hardness scales with the same names. A common scale for

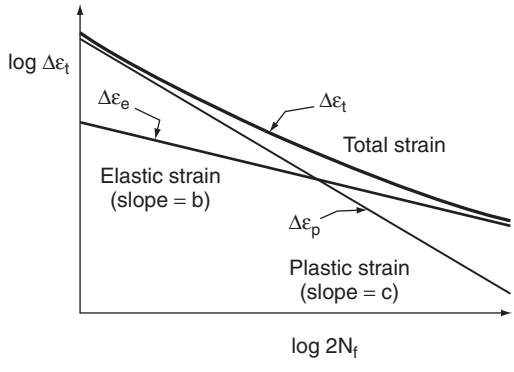

Figure W10.8. Separation of a $\Delta\varepsilon_t$–N_f fatigue curve into its elastic and plastic components.

minerals is *Mohs* hardness, determined by a scratch test, which extends from 1 for talc to 10 for diamond.

The Knoop hardness test is a microindentation test that uses an indenter in the form of an elongated pyramid while the Vickers test uses a square pyramid of diamond. The Knoop and Vickers hardnesses are defined as the ratio of the applied force or load to the surface area of the indentation. The Vickers hardness VHN is given by

$$\text{VHN} = \frac{1.854F}{d^2}, \tag{W10.24}$$

where F is the load in kilograms force (kgf) and d is the length of the diagonal of the square indentation in millimeters. Some Vickers hardness values for metals and other hard materials are given in Table 10.6. These hardness values, as with many other mechanical properties, are sensitive to processing treatments that the material may have received, especially those affecting the surface region.

The indentation of the Knoop indenter in the material under test is shallower than that of the Vickers indenter, thus making the Knoop method more appropriate for brittle materials and for thin layers. Because of the shallowness of the indentation, the surfaces of materials to be tested for Knoop hardness must be very smooth.

W10.9 Further Discussion of Hall–Petch Relation

The *Hall–Petch relation* was originally justified on the basis of the assumption that the effect of grain boundaries is to pin dislocations, but more recent interpretations emphasize the emission of dislocations by grain boundaries. An approach by Li[†] takes the onset of plastic deformation in polycrystalline materials as due to the activation of dislocation sources, which are assumed to be grain-boundary ledges. The shear yield stress for the motion of a dislocation relative to a distribution of other dislocations has been given in Eq. (W10.9) by

$$\tau_y(\rho) = \tau_y + \alpha G b \sqrt{\rho}, \tag{W10.25}$$

where ρ is the dislocation density and the other symbols are as defined earlier. If it is assumed that there is a uniform distribution of dislocation sources on the surfaces of all grain boundaries, regardless of their size, the dislocation density ρ will be proportional to S_v, the grain boundary area per unit volume. If the grains are all taken to be cubes of volume d^3, S_v will be given by

$$S_v = \frac{1}{2}\frac{6d^2}{d^3} = \frac{3}{d}, \tag{W10.26}$$

where the initial factor of $\frac{1}{2}$ accounts for the fact that each cube face (i.e., each grain boundary) is shared by two grains. The Hall–Petch relation of Eq. (10.43) is obtained when the result that $\rho \propto S_v \propto 1/d$ is used in Eq. (W10.25).

[†] J. C. M. Li, *Trans. TMS-AIME*, **227**, 239 (1963).

The yield stress can also be increased by solid-solution strengthening, as discussed in Section W10.5. The typical example is dilute alloys of C in BCC α-Fe, where $\sigma_y = \sigma_0 + k_y N_C^{1/2}$. Here N_C is the atomic fraction of C present in Fe.

W10.10 Analysis of Crack Propagation

When fracture occurs in a ductile material in which significant amounts of plastic deformation can occur, the critical stress will be increased above the prediction of Eq. (10.48) since the strain energy required for the generation of plastic deformation near the crack must be included. Plastic deformation of the material surrounding the crack tip can take the form of a dense array of dislocations and microcracks whose presence can slow down and even stop the propagation of the crack. The effective surface energy γ_p associated with the plastic deformation is equal to the work per unit area required to carry out the plastic deformation. When γ_p is added to γ_s in Eq. (10.48), *Griffith's criterion* in its general form becomes

$$\sigma_c = \sqrt{\frac{(2\gamma_s + \gamma_p)E}{\pi a}}. \tag{W10.27}$$

For many ductile materials $\gamma_p \gg \gamma_s$, so that

$$\sigma_c = \sqrt{\frac{\gamma_p E}{\pi a}} \tag{W10.28}$$

for the case of ductile fracture. The effect of the plastic deformation is to blunt the crack tip, thus relaxing the stress concentration there by increasing the local radius of curvature. As a result, ductile fracture requires higher stress levels than brittle fracture.

Correlations of *fracture toughness* K_{1c} with density ρ, Young's modulus E, and with strength σ_f for several classes of engineering materials (alloys, plastics, elastomers, composites, ceramics, glasses, etc.) have been presented by Ashby in the form of materials property charts.[†] These charts and the accompanying discussions are helpful in that they present and condense a large body of information and reveal correlations between the properties of materials. A striking feature of the charts is the clustering of members of a given class of materials. This clustering and the relative positions of the various clusters on the charts can be understood in terms of the type of bonding, the density of atoms, and so on, in the materials. Within each cluster the position of a given material can be influenced by the synthesis and processing that it receives. The following charts are also presented by Ashby: E versus ρ, σ_f versus ρ, E versus σ_f, and E/ρ versus σ_f/ρ.

The rate of elastic strain energy release by a crack is $G(\text{el})$, defined by

$$G(\text{el}) = -\frac{1}{2d}\frac{\partial \Delta U_{\text{el}}}{\partial a} = \frac{\pi \sigma^2 a}{E}. \tag{W10.29}$$

[†] M. F. Ashby, Materials Property Charts, in *ASM Handbook*, Vol. 20, ASM International, Materials Park, Ohio, 1997.

At the point of fracture $G(\text{el}) = G_c(\text{el})$ and the critical fracture stress can therefore be expressed in terms of $G_c(\text{el})$ by

$$\sigma_c = \sqrt{\frac{EG_c(\text{el})}{\pi a}}. \tag{W10.30}$$

By comparing this result with Eqs. (W10.27) and (10.49), it can be seen that

$$K_c = \sqrt{EG_c(\text{el})}. \tag{W10.31}$$

The quantity $G_c(\text{el})$ is also known as the *critical crack extension force*, with units of N/m.

REFERENCE

Gilman, J. J., *Micromechanics of Flow in Solids*, McGraw-Hill, New York, 1969.

PROBLEMS

W10.1 A bar of a solid material undergoes two consecutive deformations along the x axis corresponding to nominal normal strains ε_1 and ε_2, as defined by $\varepsilon_1 = (x_1 - x_0)/x_0$ and $\varepsilon_2 = (x_2 - x_1)/x_1$.

(a) Show that these two nominal strains are not additive [i.e., that $\varepsilon_{\text{total}} = (x_2 - x_0)/x_0 \neq \varepsilon_1 + \varepsilon_2$].

(b) Show, however, that the corresponding true strains $\varepsilon_{\text{true}}(1)$ and $\varepsilon_{\text{true}}(2)$, as defined in Eq. (10.8), are additive.

(c) Find the difference between ε and $\varepsilon_{\text{true}}$ for $\Delta l = 0.1 l_0$.

W10.2 From the expressions given for the shear modulus G and the bulk modulus B in Table 10.4, show that Poisson's ratio ν for an isotropic solid must satisfy $-1 < \nu < \frac{1}{2}$.

W10.3 Derive the expression for the elastic energy density $u_{\text{el}}(\varepsilon)$ for a cubic crystal given in Eq. (10.32).

W10.4 Using the general definitions for strains as $\varepsilon_1 = \partial u_x/\partial x$, $\varepsilon_5 = \partial u_x/\partial z + \partial u_z/\partial x$, and so on, show that the equation of motion, Eq. (10.35), can be written as the wave equation given in Eq. (10.36).

W10.5 Consider the values of E, G, B, and ν given in Table 10.2 for several polycrystalline cubic metals.

(a) Show that the values of E, G, and ν are consistent with the expressions for isotropic materials given in Table 10.4.

(b) Show that the same cannot be said for the values of B.

W10.6 If the changes in stress and strain in a material occur so rapidly (e.g., at sufficiently high frequencies) that no relaxation occurs, show that the stress/strain ratio is given by the unrelaxed elastic modulus, $E_u = E_r \tau_\sigma / \tau_\varepsilon$.

W10.7 **(a)** For the conditions shown in Fig. 10.9*a* after relaxation has occurred, derive the solutions of Eq. (W10.3) presented in Eq. (W10.4).

(b) Also derive the analogous equations for the time dependence of σ for the conditions shown in Fig. 10.9*b*.

W10.8 Let σ_0 be real and set $\varepsilon_0 = \varepsilon_{00}e^{-i\phi}$ in Eq. (W10.5) so that the strain $\varepsilon(t)$ lags behind the stress $\sigma(t)$ by a phase angle ϕ. Using these expressions (i.e., $\sigma(t) = \sigma_0 \exp(-i\omega t)$ and $\varepsilon(t) = \varepsilon_{00} \exp[-i(\omega t + \phi)]$), in Eq. (W10.6), show that $\tan\phi$ is given by Eq. (W10.8).

W10.9 The relaxation time τ for a piece of cross-linked natural rubber is 30 days at $T = 300$ K.

(a) If the stress applied to the rubber at $T = 300$ K is initially 1 MPa, how long will it take for the stress to relax to 0.5 MPa?

(b) If the relaxation time for the rubber at $T = 310$ K is 20 days, what is the activation energy E_a for the relaxation process? See Eq. (10.41) for the definition of E_a.

W10.10 Repeat Problem 10.9 for the (0001), (1100), and $(10\bar{1}0)$ planes of HCP Cd and for the three $\langle 11\bar{2}0\rangle$ directions in the (0001) plane.